

## Validity of IWFR to reconstruct an Exit Surface Wave

K. Ishizuka

HREM Research Inc, Higashimatsuyama, Saitama 355-0055, Japan

Allen et al. introduced an iterative wave function reconstruction scheme a couple of years ago [1]. This method finds an atomic-resolution wave function at the specimen exit surface based on the Gerchberg-Saxton type iteration using not a diffraction and image intensity pair, but a set of through-focus image intensities. Using this method a set of five images is normally sufficient to get a reasonably good exit wave, contrary to other methods such as the maximum likelihood method [2] or the Wiener filter method [3], which usually requires about twenty images. This method was successfully implemented as a plug-in [4] called IWFR for DigitalMicrograph [5]. Allen et al. starts the iteration with a set of wave functions, which are constructed from image *amplitudes* at observed planes and *constant (null) phases* at all the planes [1]. Each wave function is back-propagated to the nominal exit plane, and an average for these back-propagated waves gives a new estimate of the exit wave function (EWF). Then, the estimated EWF is propagated to each observed plane, and a new set of wave functions is constructed by keeping the phases but replacing the amplitudes by an observed ones. These updated wave functions are next back-propagated to the exit plane, and the iteration will continue until an estimated EWF converges. Surprisingly an estimated phase distribution at the first cycle of iteration usually demonstrates all the features of the final result. This means that our initial guess to start the Gerchberg-Saxton iteration is extremely good.

This is explained by extending the spectral analysis of in-line hologram given by Guigay [6]. We will write image amplitude downstream of the object by a distance  $z$ :

$$\psi_z(x) = \psi_0(x) \otimes p_z(x) = (1 + \phi(x)) \otimes p_z(x) \quad (1)$$

where  $\psi_0$  is an EWF ( $z=0$ ) and  $p_z$  a propagator for a distance  $z$ . Then, a Fourier transform of the intensity is given [6]:

$$I_z(u) = FT(\psi_z \cdot \bar{\psi}_z) = \delta(u) + \exp(-i\pi\lambda z u^2) \cdot \Phi(u) + \exp(+i\pi\lambda z u^2) \cdot \bar{\Phi}(-u) + \exp(-i\pi\lambda z u^2) \int \exp(i2\pi x u) \phi(x) \bar{\phi}(x - \lambda z u) dx \quad (2)$$

The process of back-propagation in Fourier space corresponds to multiplying by  $\exp(+i\pi\lambda z u^2)$ , which is a well-known defocusing factor in electron microscopy. Then, Eq. (2) reduces to

$$R_z(u) = I_z(u) \cdot \exp(+i\pi\lambda z u^2) = \delta(u) + \Phi(u) + \exp(+i2\pi\lambda z u^2) \cdot \bar{\Phi}(-u) + \int \exp(i2\pi x u) \phi(x) \bar{\phi}(x - \lambda z u) dx \quad (3)$$

As you may note the second and third terms in this expression correspond to an object spectrum  $\Phi(u)$  and its conjugate spectrum, respectively. An average for back-propagated intensities of a set of  $N$  focal series with a defocus step  $\epsilon$  becomes

$$R(u) = \frac{1}{N} \sum_j R_{z_j}(u) = \delta(u) + \Phi(u) + \left\{ \frac{1}{N} \sum_j \exp(+i2\pi\lambda z_j u^2) \right\} \cdot \bar{\Phi}(-u) + \int \exp(i2\pi x u) \phi(x) \left\{ \frac{1}{N} \sum_j \bar{\phi}(x - \lambda z_j u) \right\} dx \quad (4)$$

Thus, the object spectrum adds up coherently, while the conjugate term adds up destructively. The weighting factor for the conjugate term will be transformed to

$$\begin{aligned} \frac{1}{N} \sum_j \exp(+i2\pi\lambda z_j u^2) &= \frac{1}{N} \exp\{+i\pi\lambda(z_0 + z_{N-1})u^2\} \frac{\sin(\pi\lambda N\epsilon u^2)}{\sin(\pi\lambda\epsilon u^2)} \\ &= \exp\{+i\pi\lambda(z_0 + z_{N-1})u^2\} L(\lambda\epsilon u^2) \end{aligned} \quad (5)$$

Here,  $L(x)$  has the same form of the Laue function used in x-ray crystallography, which becomes unity for integral  $x$ . Although the conjugate term for integral  $\lambda\epsilon u^2$  adds up coherently, its contribution is scrambled by the preceding phase term. The contribution from the forth term is small for a weak scattering object. Even for a strong scattering object, its contribution may be small, if a displacement  $\lambda z u$  is larger than an object detail.

When there are wave aberrations, we can include them in the equations above. Here, we replace  $\phi(x)$  in Eq. (1) with  $\phi'(x)$  that is affected by all the aberrations except defocusing. When we correct the aberrations on the back-propagated intensities, Eq. (4) becomes

$$\begin{aligned} R(u) &= \delta(u) + \Phi(u) + \left\{ \frac{1}{N} \sum_j \exp(+i2\pi\lambda z_j u^2) \right\} \cdot \exp\{i2\chi'(u)\} \bar{\Phi}(-u) \\ &+ \int \exp(i2\pi x u) \phi'(x) \left\{ \frac{1}{N} \sum_j \bar{\phi}'(x - \lambda z_j u) \right\} dx \end{aligned} \quad (6)$$

Here,  $\chi'(u)$  is a wave aberration function that includes all the aberrations except defocusing. Thus, the conjugate term suffers from doubled aberration, and its contribution to the estimated EWF will further decrease. In conclusion, we can estimate the object spectrum  $\Phi(u)$  from an average for FT's of back-propagated *intensities* without knowing any phase information. This verifies the first step of IWFR, where the EWF (the object spectrum) is estimated from an average for FT's of back-propagated *amplitudes*. However, Eq. (4) shows that the object spectrum may be estimated more reliably from observed *intensities* than from *amplitudes*. This is verified in Fig. 1 using five images from a set of Si<sub>3</sub>N<sub>4</sub> through-focus images obtained with a Philips CM300-FEG at NCEM.

- [1] L.J. Allen, W. McBride, N.L. O'Leary, M.P. Oxley, *Ultramicroscopy* 100 (2004) 91.
- [2] W.M.J. Coene, A. Thust, M. Op de Beek, D. Van Dyck, *Ultramicroscopy* 64 (1996) 109.
- [3] R.R. Meyer, A.I. Kirkland, W.O. Saxton, *Ultramicroscopy* 92 (2002) 89.
- [4] A IWFR plug-in for DigitalMicrograph (Gatan Inc), see [www.hremresearch.com](http://www.hremresearch.com).
- [5] Gatan Inc., see [www.gatan.com](http://www.gatan.com)
- [6] J.P. Guigay, *Optik* 49 (1977) 121.
- [7] The author greatly acknowledges Dr. Christian Kisielowski for providing the Si<sub>3</sub>N<sub>4</sub> data.

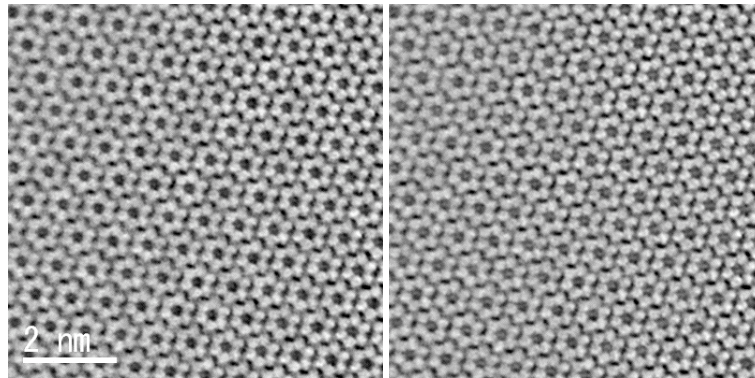


Fig. 1 Phase distributions at (left) the first cycle and (right) the last (fifth) cycle.